SARS-CoV-2 Virus Detection Via a Polymeric Nanochannel-Based Electrochemical Biosensor

Amane Shiohara, Marcin Wojnilowicz, Quanxia Lyu, Yi Pei, Christopher D. Easton, Yu Chen, Jacinta F White, Alexander McAuley, Beatriz Prieto-Simon, Helmut Thissen, and Nicolas H Voelcker*

The development of simple, cost-effective, rapid, and quantitative diagnostic tools remains critical to monitor infectious COVID-19 disease. Although numerous diagnostic platforms, including rapid antigen tests, are developed and used, they suffer from limited accuracy, especially when tested with asymptomatic patients. Here, a unique approach to fabricate a nanochannel-based electrochemical biosensor that can detect the entire virion instead of virus fragments, is demonstrated. The sensing platform has uniform nanoscale channels created by the convective assembly of polystyrene (PS) beads on gold electrodes. The PS beads are then functionalized with bioreceptors while the gold surface is endowed with anti-fouling properties. When added to the biosensor, SARS-CoV-2 virus particles block the nanochannels by specific binding to the bioreceptors. The nanochannel blockage hinders the diffusion of a redox probe; and thus, allows quantification of the viral load by measuring the changes in the oxidation current before and after virus incubation. The biosensor shows a low limit of detection of ≈1.0 viral particle mL^{-1} with a wide detection range up to 10^8 particles mL^{-1} in cell culture media. Moreover, the biosensor is able to differentiate saliva samples with SARS-CoV-2 from those without, demonstrating the potential of this technology for translation into a point-of-care biosensor product.

1. Introduction

Biosensors enabling the detection of pathogens are in high demand worldwide. Rapid, accurate, simple, and cost-efficient biosensors are desired to enable improved detection of emerging infectious diseases and are a prerequisite for the

improved management of outbreaks. The importance of biosensors in the context of viral infectious diseases has been thrust in the spotlight by the COVID-19 pandemic. COVID-19 is a human infectious disease caused by a newly emerged human coronavirus, severe acute respiratory syndrome coronavirus 2 (SARS-CoV-2).[1] The current gold standard for SARS-CoV-2 detection is reverse transcription polymerase chain reaction (RT-PCR).[2] Although PCR can offer high reproducibility and reliability due to its ability to detect at the genomic level, it requires complex sample preparation steps to extract genetic material; thus, incurring high labor costs.[3,4] Moreover, PCR tests are unable to discriminate between active infections and post-infection states after recovery, when non-contagious viral RNA fragments may still be present in the specimen collected, causing false-positive test results.

As alternatives to PCR tests, antigen-based and antibody-based rapid point-of-care (POC) diagnostic approaches have been developed. These tests can remove the burden of transporting clinical samples to laboratories and provide the results much quicker than PCR tests.[5] However, these rapid antigen or antibody-based tests suffer from a much lower accuracy compared to PCR tests, frequently leading to false negative and false positive results.[6,7] As such, a point-of-care diagnostic approach that is rapid, highly sensitive, and can

A. Shiohara, M. Wojnilowicz, Y. Pei, N. H. Voelcker
Drug Delivery, Deposition, and Dynamics
Monash Institute of Pharmaceutical Sciences
Monash University
Parkville, Victoria 3052, Australia
E-mail: nicolas.voelcker@monash.edu

A. Shiohara, M. Wojnilowicz, Q. Lyu, Y. Pei, C. D. Easton, Y. Chen,
J. F. White, A. McAuley, H. Thissen, N. H. Voelcker
Commonwealth Scientific and Industrial Research Organisation (CSIRO)
Clayton, Victoria 3168, Australia
A. Shiohara, N. H. Voelcker
Melbourne Centre of Nanofabrication
Victorian Node of the Australian National Fabrication Facility
Clayton, Victoria 3168, Australia
B. Prieto-Simon
Department of Electronic Engineering
Universitat Rovira i Virgili
Tarragona 43007, Spain
B. Prieto-Simon
ICREA
Pg. Lluís Companys 23, Barcelona 08010, Spain

**ADVANCED
SCIENCE NEWS**

www.advancedsciencenews.com

NANO · MICRO

small

www.small-journal.com

accurately detect the virus throughout the infectious period, is still highly desired.

Electrochemical biosensors have been gaining attention due to their excellent sensitivity, low production cost, user-friendly operation, short analysis time, and most of all, excellent potential to afford point-of-care detection.[2,7] Various types of electrochemical biosensors have been successfully designed and demonstrated with enhanced properties, thanks in particular to recent advancements in nanotechnology.[8] Electrochemical biosensors based on nanostructures provide a high surface area, which can result in remarkable sensitivity enhancement.[9–11] Moreover, the highly controllable nanoscale morphology makes it possible to exploit different sensing mechanisms. For instance, nanopore and nanochannel based sensors have been demonstrated to achieve highly enhanced detection sensitivity.[12] These biosensors are well suited for analytes with a size in the nanometer range, such as viruses, which can be trapped upon binding with suitable bioreceptors immobilized on the inner walls of the channels. The binding event then leads to complete or partial channel blockage, which can be monitored by the change in electrochemical signal, caused by the decreased diffusion rate of electrochemical probes. The main advantage of this detection mechanism is the ability to detect the entire viral particle, instead of the genetic components or virus fragments, increasing the accuracy in identifying contagious patients. The nanochannels can also act as a filter to remove microscale sample components such as cells.

Porous anodic alumina (pAAO) membranes are some of the commonly used materials for nanochannel-based biosensors.[13–16] De la Escosura-Muniz et. al reported the nanochannel blockage-based detection of proteins in blood samples using pAAO membranes with 200 nm pore diameter in 2011 and 2013.[14,15] In both studies, suitable bioreceptors were immobilized on the inner walls of the nanochannels. Antibody-modified pAAO membranes were then incubated with the target analytes partially blocking the nanopores of pAAO, causing changes in interferometric responses. A second incubation step with Au nanoparticle-labeled antibodies with affinity toward a different epitope on the analytes further improved the nanochannel-blocking efficiency and sensitivity of detection. In addition, nanostructured porous silicon (pSi) also represents a class of widely used materials for nanochannel-based biosensors. As an example, Reta et al. demonstrated viral detection by nanochannel-based electrochemical sensing using a porous silicon (pSi) platform.[7] A pSi layer was fabricated by electrochemical anodization of Si in hydrofluoric acid (HF) solution. The porous layer was then detached from the Si substrate and placed on an Au electrode to facilitate electrochemical sensing. Although both pAAO and pSi membrane-based sensors show excellent sensitivity and selectivity, their manufacturing process often involves hazardous chemicals such as chromic acid and HF. These membranes are brittle and hard to handle; thus, transferring them to the electrode surface can be challenging. To solve this problem, Guo. et al. stabilized the surface of freshly etched pSi via thermal hydrocarbonization (THC) and thermal carbonization (TC), which requires treating the substrate at 525 °C and 800 °C, respectively, in an acetylene atmosphere to create an ultrathin carbon layer in order to increase the electrical conductivity.[17] However, acetylene is highly flammable and can decompose explosively under high pressure.

Previously, we successfully demonstrated the ability of viral particle detection using a nanochannel-based biosensor with a monolayer of polystyrene (PS) beads (≈350 nm in diameter) to detect MS2 bacteriophage in buffer.[18] Here, we report SARS-CoV-2 virus detection in complex matrices such as cell culture media after coating the Au surface at the bottom of the nanochannels with disodium 2,2″-dithiobisethane sulfonate (MESNA), which reduces biofouling. The fabrication of the biosensor did not require any hazardous chemicals or tedious steps. The monolayer of the PS beads was generated by means of the convective assembly technique and the bioreceptors were immobilized on the bead surface through N-ethyl-N'-(3-(dimethylamino) propyl) carbodiimide/N-hydroxysuccinimide) (EDC/NHS) chemistry. A limit of detection (LOD) of ≈1.0 viral particle mL^{-1} was achieved with inactivated SARS-CoV-2 in cell culture media, which is lower than most other sensors reported previously. Importantly, the antifouling molecule protected biosensor was capable of distinguishing the SARS-CoV-2 infected saliva samples from those not containing the virus.

2. Experimental Section

2.1. Reagents and Instruments

Square glass slides (10.16 × 10.16 cm^2) coated with 12.5 nm chromium and 150 nm Au layers were purchased from Telic Company (USA) and diced into 1.5 × 2.5 cm^2 pieces with a Disco DAD321 dicing saw. Carboxylated PS beads (diameter 500 nm) were purchased from PolySciences, Inc. Disodium 2,2″-dithiobisethane sulfonate (MESNA) was purchased from AK Scientific. Potassium ferrocyanide (K$_4$[Fe(CN)$_6$]), potassium ferricyanide (K$_3$[Fe(CN)$_6$]), N-hydroxysuccinimide (NHS), 1-Ethyl-3-(3-dimethylaminopropyl)carbodiimide (EDC), sodium dodecyl sulphate (SDS), ethanolamine, phosphate buffered saline (PBS) tablets, 2-(N-morpholino)-ethanesulfonic acid (MES), tris(hydroxymethyl)aminomethane (TRIS), glycine, Tween 20, gentamycin, and amphotericin B were purchased from Sigma-Aldrich (Australia). Dulbecco's phosphate-buffered saline (1 × DPBS), Hank's Balanced Salt Solution (HBSS), fetal bovine serum, Dulbecco's Modified Eagle Medium (DMEM), goat anti-human HRP-conjugate IgG, and MagMAX-96 Viral RNA Isolation Kit were purchased from Thermofisher Scientific (Australia). CR3022 antibody was purchased from Resolving IMAGES. Polyvinylidene fluoride (PVD-F) membrane and ECL Clarity reagent were purchased from Bio-Rad (Australia). All reagents were prepared in Milli-Q water and used as received.

2.2. Preparation of Viral Inoculum

SARS-CoV-2: SARS-CoV-2 was obtained from Victorian Infectious Diseases Reference Laboratory (strain hCoV/Australia/VIC01/2020) and raised in VeroE6 cells in DMEM/HEPES media supplemented with 2% FBS and 1% gentamycin/amphotericin B for 72 h. The virus was harvested at TCID50 5 × 10^5 mL^{-1} and centrifuged at 4000 × g for 10 min at 21 °C to remove cell debris. The virus stock was inactivated using gamma-irradiation with dose of 50 kGy.

HCoV-229E: HCoV-229E was raised in human fetal lung fibroblasts MRC-5 cells in MEM media supplemented with 2%

**ADVANCED
SCIENCE NEWS**

www.advancedsciencenews.com

**NANO · MICRO
small**

www.small-journal.com

FBS and 1% gentamycin/amphotericin B for 7 days. The virus was harvested and centrifuged at $4000 \times g$ for 10 min at 21 °C to remove cell debris.

2.3. Quantitative Real-Time Polymerase Chain Reaction (RT-qPCR) of SARS-CoV-2

RNA was isolated from supernatant samples using a MagMAX-96 Viral RNA Isolation Kit on a Kingfisher Flex instrument (Thermo Fisher Scientific). SARS-CoV-2 RNA load was determined by RT-qPCR, with each sample tested in duplicate using a modified assay targeting the viral E gene: Forward primer 5′-AGTACGAACTTATGTACTCATTCGTT-3′; Probe and Reverse primer were used according to a previous study.[19] Copy numbers for individual samples were calculated using cycle threshold (C_T) values as SARS-CoV-2 E gene copies per mL, with an equation established from standard curve data using a synthetic DNA standard of known copy number.

2.4. Preparation of Viral Transport Media (VTM)

Fetal bovine serum (FBS) was heat-inactivated by incubation in water bath at 56 °C for 30 min. After that, FBS was added to Hank's Balanced Salt Solution (HBSS) to 2% final concentration of FBS and supplemented with gentamycin (100 µg mL^{-1}) and amphotericin B (0.5 µg mL^{-1}).

2.5. Preparation of Nanochannel-Based Biosensor With PS Beads

Nanochannels were created by assembling a monolayer of PS beads (diameter 500 nm) on the smooth Au surface of a glass slide sputter-coated with Au at a thickness of 150 nm, using a convective assembly technique. Specifically, 500 µL of the aqueous PS beads solution was centrifuged at 12 000 rpm for 5 min and 400 µL of the supernatant was removed followed by the addition of 3 µL of 10% sodium dodecyl sulphate (SDS) solution. The Au-coated slides were sonicated in acetone for 15 min followed by another 15 min of sonication in ethanol. After rinsing with ethanol and drying under nitrogen, the slides were treated with UV-ozone using SAMCO UV-Ozone cleaner (Model CD240-10S2, Toyozumi Dengenkiki Co Ltd) for 45 min. 5 µL of the freshly prepared PS bead suspension was deposited on the edge of the slide and the convective assembly of the PS beads was performed with C-863 Mercury DC Motor controller (Physik Instrumente [PI] GmbH & Co. KG). The PS beads were immobilized on the Au surface by annealing the slides on a hot plate at 109 °C for 3.5 min. The surface was vigorously washed with Milli-Q water and dried with a stream of nitrogen gas.

2.6. Bioreceptor Immobilization on the Surface of PS Beads

The biosensor platform fabrication process and the surface modification of the nanochannels between the PS beads are illustrated in **Scheme 1**. First, a well-ordered and closely-packed monolayer of PS beads was convectively assembled on the Au electrode. Convective assembly is a commonly used method to prepare high-quality colloidal crystals with very few defects, as confirmed by optical microscopy and scanning electron microscopy (SEM).[20] Next the PS beads were annealed on the electrode surface by heating at 109 °C for 3.5 min on a hot plate (Scheme 1a,b). Silica was deposited on the top surface of PS beads by means of glancing angle deposition technique using E-beam evaporator (Intlvac Nanochrome II) (Scheme 1c,d). The slides were tilted at 75° and deposition was performed with no rotation. Judging from the SEM images, the nanochannel diameters for the PS bead layer before and after SiO_2 coating (Scheme 1e,f) were not statistically different (Figure S1, Supporting Information). Afterward, PS beads were treated with UV-ozone for 1 min to increase the amount of carboxylic group on the commercial beads' surface. The Au-coated slides with the PS bead monolayer were mounted in a Teflon cell for electrochemical sensing and immobilization of bioreceptors was performed in the cell. 0.2 M NHS and 0.1 M EDC solutions were prepared in pH 5.5 0.2 M MES buffer, respectively. Solutions were mixed in a 1:1 volume ratio, and 100 µL was incubated on the carboxylated beads surface for 30 min at room temperature to form succinimidyl ester groups. The biosensors were washed with 0.01 M PBS three times and 100 µL of 125 µg mL^{-1} CR3022 antibody in 0.01 M PBS pH 7.4 was added to the cell and incubated overnight at 4 °C. Afterward, the surface was washed with 0.01 M PBS three times.
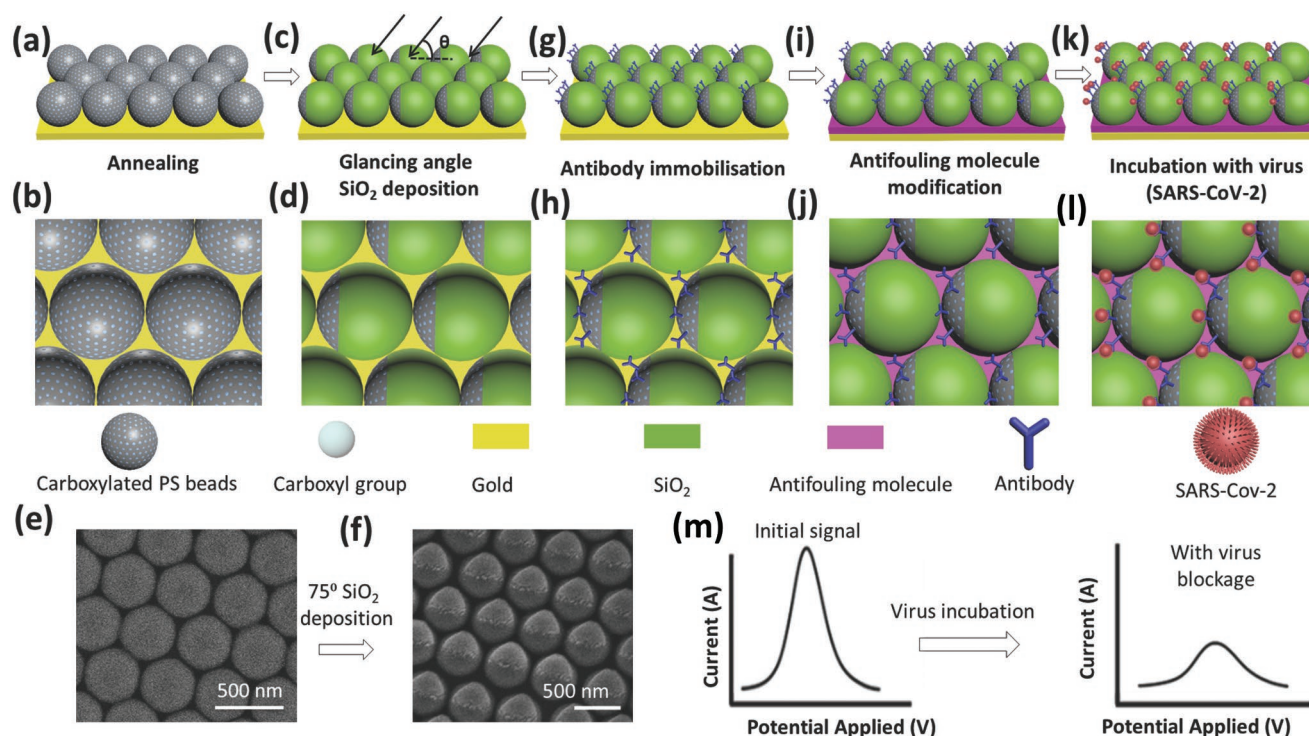
2.7. Introduction of Antifouling Molecules

After the immobilization of antibodies on the PS bead surface, the biosensor was incubated with 2.5 mM MESNA in 0.01 M PBS solution for 2 h at room temperature. The biosensor was then washed with 0.01 M PBS for three times followed by the addition of 100 µL of 0.1 M ethanolamine in 0.01 M PBS to the cell for 45 min incubation at room temperature to quench the unreacted succinimidyl ester group. The biosensor was washed again with 0.01 M PBS solution for three times and stabilized either in VIRAC transport media or cell culture media (DMEM supplemented with 2% FBS and 1% antibiotics) at room temperature before being used for analyte detection.

2.8. Biosensor Characterization

Surface modification steps were characterized by X-ray photoelectron spectroscopy (XPS). XPS analysis was performed on an AXIS Nova spectrometer (Kratos Analytical Inc., Manchester, UK) using the standard protocol detailed elsewhere.[21] The following parameters were employed during analysis: X-ray source and power: monochromated Al Kα source at 180 W; system pressure: between 10^{-9} and 10^{-8} mbar; Pass energy: 160 eV (survey) and 20 eV; Step size: 0.5 eV (survey) and 0.1 eV (high resolution); emission angle: 0° as measured from the surface normal; charge neutralizer: on.

Data processing was performed using CasaXPS processing software version 2.3.15 (Casa Software Ltd., Teignmouth, UK). The atomic percentages (at%) of the detected elements

**ADVANCED
SCIENCE NEWS**

www.advancedsciencenews.com

NANO · MICRO

small

www.small-journal.com

Scheme 1. Schematic illustration of the fabrication and detection process of the nanochannel-based electrochemical biosensors. a) Side view and b) top view of annealed carboxylated PS beads on the gold electrode at 109 °C for 3.5 min. c) Side view and d) top view of deposited SiO$_2$ at an angle of 75° on the annealed PS beads. e) SEM image of annealed PS beads on the gold electrode. f) SEM image of deposited SiO$_2$ at an angle of 75° on the annealed PS beads. g) Side view and h) top view of SARS-CoV-2 antibodies immobilized on PS beads with exposed carboxyl groups. i) Side view and j) top view of antifouling molecules modified gold electrode. k) Side view and l) top view of the SARS-CoV-2 virus bound on the electrode, blocking the nanochannels and inducing a decrease in the electrochemical signal. m) Mechanism of the fabricated nanochannel-based biosensor to detect the SARS-Cov-2 virus by means of differential pulse voltammetry (DPV).

were calculated using integral peak intensities and the sensitivity factors supplied by the manufacturer. Binding energies were referenced to the C 1 s peak at 284.7 eV for aromatic hydrocarbon.

Scanning electron microscopy (SEM) was performed to characterize the morphology of the surface of the biosensor. Images of the PS beads were taken after each fabrication step, annealing, and silica deposition. All images were obtained using an FEI NovaNano SEM 430.

2.9. Sandwich Assay

Biosensing platforms with or without conjugated CR3022 antibody were first passivated with 5% BSA solution in D-PBS for 1 h, washed trice with D-PBS, and then incubated for 45 min with either 100 µL of SARS-CoV-2 viral inoculum or 100 µL of 5 µg mL^{-1} goat anti-human IgG (blocking antibody) or without additional analyte. After this, the biosensing platforms were washed three times with D-PBS and 100 µL of 5 µg mL^{-1} CR3022 antibody was added for 1 h as a primary antibody, followed by incubation of all samples with goat anti-human HRP-conjugate IgG (detection antibody) for 30 min. The chemiluminescence signal was induced with ECL Clarity reagent and read using an iBright FL1500 Imaging System (Thermofisher, US).

2.10. Electrochemical Detection

Solutions of SARS-CoV-2 virus were prepared by serially diluting the stock viral inoculum either with DPBS or cell culture media. The virus detection without MESNA modification was performed on the serially diluted viral inoculum with DPBS at dilution factors of 50×, 20×, 10×, 5×, and 1×. For the detection with the biosensors modified with MESNA, the viral titre was adjusted to 10^0, 10^2, 10^4, 10^6, and 10^8 viral particles mL^{-1}. In both experiments, 100 µL of each solution was incubated on the sensor surface for 45 min at room temperature with mild agitation. After each incubation, the electrode was washed with 1× DPBS for three times to remove unbound viral particles. Voltammograms prior to and after virus incubation were obtained to determine the nanochannel blockage, monitoring the oxidation current intensity of the selected potential range, which reflected the diffusion change of the redox probe. For the measurement, each electrode was immersed in 850 µL of 2 mM K$_4$[Fe(CN)$_6$] and 2 mM K$_3$[Fe(CN)$_6$] mixture solution prepared in 0.01 M PBS. The voltammograms were obtained by scanning the potential from 0 to 0.7 V. All electrochemical measurements were conducted with an electrochemical analyzer (Autolab potentiostat) using a three-electrode system. A custom-designed Teflon cell was assembled to host the modified Au slide as the working electrode, silver/silver chloride as the reference electrode, and a platinum wire as the counter electrode

ADVANCED
SCIENCE NEWS

www.advancedsciencenews.com

NANO · MICRO
small
www.small-journal.com

(Figure S2, Supporting Information). Selectivity measurement was performed to validate the function of the biosensor. The biosensor was challenged with either T4 bacteriophages[22] or human 229E coronavirus (HCoV-229E),[23] which have similar size and shape to the target analyte, SARS-CoV-2 virus. To compare sensitivity, the current intensity values were normalized as follows: $\Delta I = (I_0 - I)/I_0$, where ΔI is the normalized current difference between I_0, the initial current intensity prior to analyte incubation and I, the current intensity after the incubation with the analyte. Human saliva samples were collected from human healthy donors under CSIRO Human Research Ethics application (approval no. 2020_078_HREC). The collected saliva samples were divided into two groups with one group spiked with SARS-CoV-2 virus (positive samples) and the other group untreated (negative samples). The two groups of saliva samples were first filtered by filter paper with a pore size of ≈1–3 µm (Whatman), and then, filtered by filters having a pore size of 0.45 µm subsequently. The filtered saliva samples were then diluted by 0.01 M PBS (1:1 v/v) before being used for measurements with the biosensor.

2.11. Immunochemiluminescence Dot Blot Assay

PVD-F membranes were activated with 100% methanol for 15 s, followed by derivatization in water and TRIS/glycine buffer for 5 min each. Membranes were dried from excess buffer and 2 µL of each sample was loaded. The membranes were then left to air-dry for 30 min, washed twice with 0.1% Tween 20 in PBS (PBS-T) under agitation for 5 min each, and blocked with 5% skim milk buffer (skim milk powder in PBS-T) for 1 h. After this, membranes were washed trice with PBS-T (5 min each) and 1:5000 dilution of anti-SARS-CoV-2 spike glycoprotein S1 monoclonal antibody (CR3022 clone) in 1% BSA in PBS-T was added for 1.5 h. The membranes were then washed again twice in PBS-T and 1:5000 dilution of detection antibody (goat anti-human HRP-conjugate IgG) was added and incubated for 1 h. Chemiluminescence signal was detected using ECL Clarity reagent (BioRad) as described by the manufacturer's protocol and imaged using iBright FL1500 Imaging System (Thermofisher, US).

2.12. Ratiometric Transmission Electron Microscopy (TEM) Imaging

200-mesh copper grids coated with carbon film (EMSCF200H-CU-TH ProSciTech, Qld, Australia) were glow discharge treated in a nitrogen atmosphere using a Pelco easiGlow (Ted Pella Inc, CA, USA) to render the grids hydrophilic.

To quantify the concentration of the stock virus solution, a counting method was designed as follows. First, a PS nanoparticle dispersion 0.1%, 0.1 µm (ProSciTech SL0.1S Qld, Australia) was diluted at the ratio of 1:100 using Milli-Q from stock $(1.818 \times 10^{12}$ particles per mL) to give a working concentration of 1.818×10^{10} nanoparticles per mL. Then, the stock virus solution (the concentration of which needed to be quantified) was mixed 1:1 (v:v) with this prepared PS nanoparticle working solution. 2 µL of this mixture was applied to the glow-discharged grid for 1 min, the excess fluid was wicked away using filter paper, and the grid washed twice with 2 µL Milli-Q water, stained with 2% phosphotungstic acid pH 6.9 by two steps with a first 4 µL application of the staining solution for 10 s and a second 4 µL application of the staining solution for 2 s to enhance the staining; then the excess liquid was wicked away with filter paper and allowed to air dry.

The PS nanoparticles and the virus particles were manually counted to give a relative quantity of virus as compared to the synthetic nanoparticles over three grids. The samples were examined using Tecnai 12 Transmission Electron Microscope (FEI, Eindhoven, The Netherlands) at an operating voltage of 120 kV. Images were recorded using a FEI Eagle 4 k × 4 k CCD camera and AnalySIS v3.2 camera control software (Olympus.)

2.13. Statistical Analysis

Data in each group were first assessed by the normality test. Data are presented as mean ± SD. Sample size is three for the statistical analysis. One-way ANOVA was used to assess the significant differences. OriginPro 2021b software was used for the statistical analysis.

3. Results and Discussion

3.1. Nanochannel Characterization

The biosensor was fabricated starting by convective assembly of a monolayer of PS beads (500 nm in diameter) on glass slides sputtered with Au (150 nm in thickness). The spaces created between the close-packed PS beads (131 ± 21 nm) were used as nanochannels to capture intact virions, which resulted in partial nanochannel blockage and a decrease in the electrochemical potential of the redox probe added to the electrochemical cells. The PS beads were partially annealed to the Au surface prior to glancing angle deposition of silica. The annealing parameters were optimized to maintain the morphology of the nanochannels. Scheme 1e,f shows the SEM images of the monolayer of PS beads before and after silica deposition. As shown in Scheme 1c,d, the top surface of the PS beads was partially coated with silica, enabling site-specific immobilization of antibodies within the nanochannels and maximizing the virus attachment inside the nanochannels. This passivation approach can reduce the chance of viruses binding on the top surface of the PS beads; thus, increasing sensitivity.[18] Afterward, carboxylic groups were introduced on the PS surface via UV-ozone treatment,[24,25] which were in turn used to attach anti-SARS-CoV-2 spike glycoprotein S1 monoclonal antibody (CR3022 clone) as a bioreceptor within the nanochannels (Scheme 1g,h). The 125 ± 30 nm diameter of the nanochannels after silica deposition and UV-ozone treatment, should allow the virus particles (≈100 nm in diameter) to diffuse into the channels and bind to the antibody immobilized on the channel walls (Scheme 1k,l).[26,27] Based on the changes in detection signal before and after SAR-Cov-2 virus incubation of the antibody-functionalized nanochannels by means of differential pulse voltammetry (DPV) method, quantitative analysis of SARS-Cov-2 virus can be achieved (Scheme 1m). In our previous work,[18]

we used smaller PS beads with a diameter at 350 nm which generated smaller nanochannels that were suitable for MS2 bacteriophage (≈23–28 nm in diameter) detection but not for SARS-CoV-2.

The surface modification steps including the attachment of the bioreceptors were characterized by means of XPS. The introduction of carboxylic groups by surface modification using the UV-ozone treatment was confirmed via survey spectra and the increase in the O/C ratio. Furthermore, this was confirmed by C1s high resolution spectra and the increase in the C5 component (O−C=O) (Table S1 and Figure S3, Supporting Information). Based on these results, a treatment time of 1 min was selected for all subsequent experiments.

XPS was also used to demonstrate the ability to use the introduced carboxylic acid groups for the covalent immobilization of proteins via an EDC/NHS reaction (Table S2 and Figure S4, Supporting Information). Using streptavidin as a model protein, we demonstrated that the N/C ratio was increased significantly after covalent immobilization using this method compared to the N/C values obtained for adsorbed protein both before and after UV-ozone treatment.

This significant increase in the N/C ratio was also observed after covalent immobilization of the CR3022 antibody via the EDC/NHS chemistry on the sensing platform (Table S3 and Figure S5, Supporting Information). These results demonstrate that the CR3022 antibody was present on the surface after surface conjugation, and that the covalent immobilization via the EDC/NHS chemistry is advantageous compared to adsorption.

To further demonstrate successful conjugation of functional CR3022 antibody to the sensing platform, we performed so called "sandwich assay" that mimics the standard ELISA protocol but was carried out on the biosensing platform (Figure S6, Supporting Information). The biosensors without (sample 1) or with (samples 2–4) attached CR3022 antibody were incubated with SARS-CoV-2 sample, blocking antibody (anti-human IgG), or detection antibody (goat anti-human HRP-conjugated antibody). No chemiluminescence signal was detected for sample without bioreceptor but treated with SARS-CoV-2 (sample 1). Conversely, chemiluminescence signal was observed for the samples with immobilized CR3022 antibody. Moreover, the signal detected in the sample treated with SARS-CoV-2 (sample 3) was higher than for bioreceptor only (sample 2), demonstrating that CR3022 antibody retains its activity after conjugation. Blocking of the bioreceptor with anti-human IgG (sample 4) resulted in significant decrease in the chemiluminescence signal, showing that the interactions between biosensor and SARS-CoV-2 virions are governed by activity of the bioreceptor. Taken together with data obtained by XPS, these results demonstrate successful conjugation of active CR3022 antibody to the biosensor.

3.2. Detection of SARS-CoV-2 Virus

Next, we determined the affinity and selectivity of applied bioreceptor using a dot blot immunoassay technique. Dilutions of SARS-CoV-2 titre in DPBS as an experimental group and virus culture media itself as a control group (DMEM supplemented with 2% FBS and 1% antibiotic/antimycotic) were immobilized on a PVDF membrane and detected with CR3022 antibody. As shown in Figure S7, Supporting Information, we observed a strong chemiluminescence signal from the undiluted SARS-CoV-2 sample, which gradually decreased as the sample became more diluted. On the contrary, the virus culture media itself showed minimal chemiluminescence signal. To further test the selectivity of the CR3022 antibody, the dot blot assay was performed with immobilized T4 bacteriophage (Figure S8, Supporting Information) and HCoV-229E (Figure S9, Supporting Information), showing insignificant interactions of CR3022 antibody with both viruses. These data demonstrate the high specificity of the CR3022 antibody toward SARS-CoV-2 but not to media components or other viruses.

As a proof of concept, detection of SARS-CoV-2 was attempted on the nanochannel biosensor surface with the immobilized CR3022 antibody. Biosensors were consecutively incubated with various concentrations of SARS-CoV-2 titre diluted with DPBS from the lowest to the highest. To assess the effect of the cell culture media, the same serial dilutions of the virus culture media were prepared and incubated with the same biosensor alongside with the virus inoculum. We also investigated the selectivity of the sensor with T4 bacteriophages. As seen in **Figure 1**, gradual decreases in oxidation current were observed in all cases as the dilution factor decreased. Taken together with the data obtained from the dot blot assay, the drop in the current for the virus culture media only and T4 bacteriophage is likely due to the biofouling effect of the media components non-specifically adsorbing on the surface of the working electrode (the Au surface). However, at the quantitative level, a significant difference in the dosage response curve between the SARS-CoV-2 samples and the other two control samples (blank cell culture media and T4 phage) was observed at lower dilutions (5× and 1×), demonstrating promising specificity of the biosensor to SARS-CoV-2.

3.3. Evaluation of Anti-Fouling Properties

As the above experiments demonstrate, the signal of the channel blockage electrochemical biosensor is also influenced by foulants that attach to the Au electrode via nonspecific absorption. The foulants can reduce the area of electrode surface that is available to the electrolytes, causing a decrease of the DPV signal. One strategy to minimize the fouling effect is to introduce antifouling coatings on the electrode surface. Self-assembled monolayers in particular have been proven to be an excellent choice for this purpose.[28–32] Here, we have chosen a self-assembled monolayer of sodium 2-mercaptoethane sulfonate (MESNA) to modify the Au electrodes due to MESNA's bifunctional properties: 1) with the thiol group to anchor on the Au electrodes and 2) with the sulfonate group to enhance the wettability of the Au surfaces; and therefore, effectively reduce biofouling.[33]

To evaluate the antifouling properties after MESNA modification, 10% fetal bovine serum (FBS) was used as the foulant. FBS attached to the surface of Au electrode after 1 h incubation at room temperature, decreasing the DPV signal (**Figure 2**a), whereas the DPV signal only dropped slightly for the MESNA modified Au electrode (Figure 2b). The use of MESNA significantly reduced the nonspecific absorption of FBS on the Au
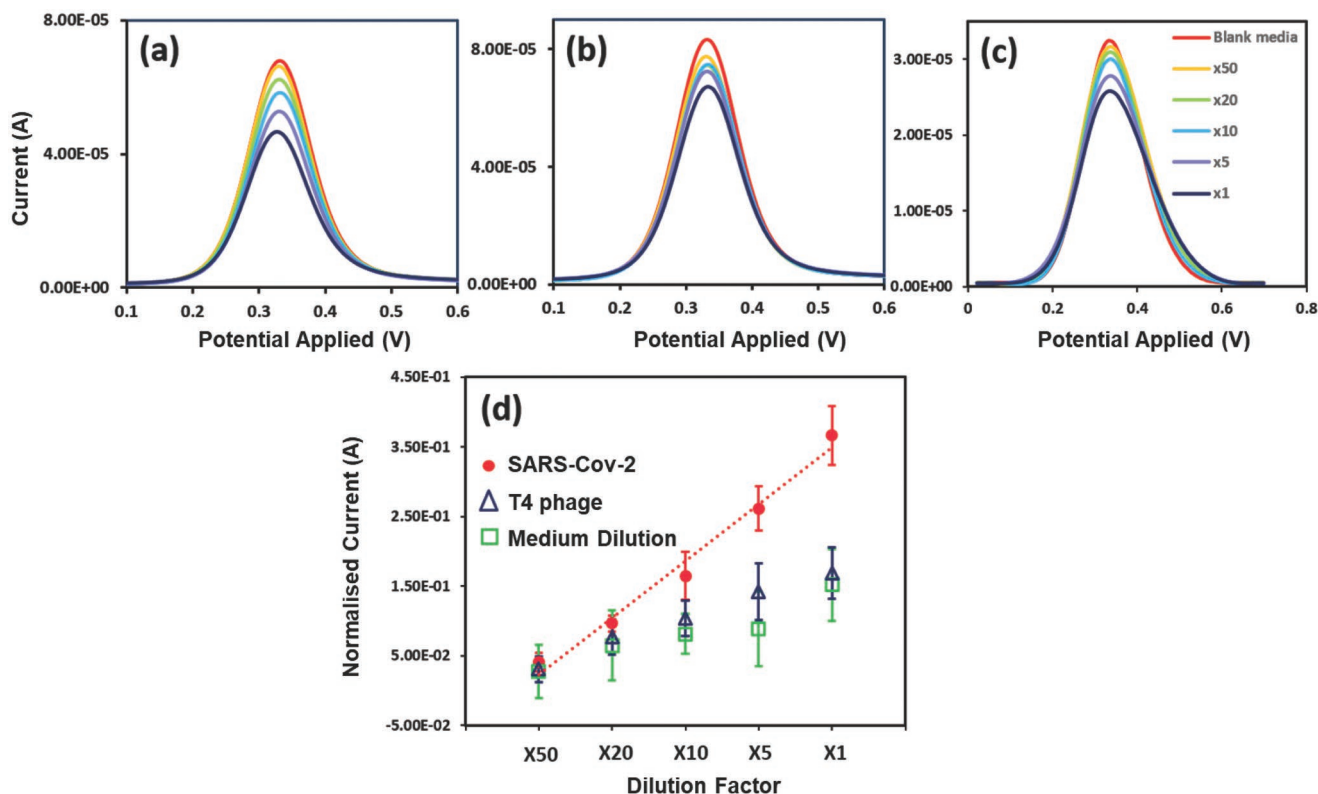
Figure 1. Differential pulse voltammograms (DPVs) of the biosensor upon consecutive incubations of a) SARS-CoV-2 virus inoculum in cell culture medium, b) blank cell culture media, and c) T4 phage virus inoculum in cell culture medium. All the three groups were diluted with 1× PBS at a dilution factor of 50×, 20×, 10×, 5×, and 1×, respectively. d) Dosage response curves of the biosensors incubated with consecutive dilutions of SARS-CoV-2 inoculum, T4 phage, and blank cell culture media with 1× PBS at a dilution factor of 50×, 20×, 10×, 5×, and 1×, respectively.

electrode. When the differences of DPV signal were normalized against the initial DPV signal, the MESNA-modified Au electrode showed a decrease of 7.19% ± 3.79% in DPV signal while bare Au electrodes showed a decrease of 80.64% ± 1.71% (Figure 2c). These results indicate that the use of MESNA can significantly improve the antifouling properties of the Au electrode; and therefore, enhance electrode stability in the presence of foulants.

The MESNA modification was then introduced to the Au surface with the PS monolayer. Similarly, the platforms modified by MESNA demonstrated a less pronounced DPV signal decrease after FBS incubation (19.50% ± 5.04%) compared to the absence of MESNA (63.45% ± 4.83%) (Figure 2d–f). The improvement resulting from the antifouling properties was not as obvious compared to flat Au surfaces. This is possibly due to the existence of the PS beads on the Au electrode. On the one hand, PS beads serve as a membrane that keeps some of the foulants out of the Au electrode. On the other hand, foulants that attach to the channel surface may hinder the diffusion of electrolyte, leading to a decrease of DPV signal.

3.4. Quantification of SARS-CoV-2 Virus Particles

To characterize the performance of the developed biosensor, an absolute concentration of the SARS-Cov-2 virus titre needed to be determined. We constructed a standard curve based on a real-time

quantitative reverse transcription polymerase chain reaction (qRT-PCR) experiment, where the known number of viral genomes was present in the sample and compared with the SARS-Cov-2 virus (Figure S10, Supporting Information). For the particular SARS-CoV-2 sample we used, a C_T value of 16 was obtained, which corresponds to $\approx 2.2 \times 10^{10}$ RNA copies per mL. Although qRT-PCR is a sensitive method for determining the virus concentration, it also accounts for the damaged and disintegrated virions that may result from sample processing and γ-irradiation, which are less likely to be detected with the proposed biosensor. Instead, we applied a ratiometric technique based on TEM imaging, where we mixed equal volumes of 100 nm diameter PS nanoparticles (1.81×10^{10} particles per mL) and SARS-CoV-2 titre. Around 130 images in total were taken during three independent experiments and manually analyzed (Figure S11, Supporting Information). We identified 376 SARS-CoV-2 particles and 1118 PS nanoparticles in total, and 5 HCoV-229E particles and 784 PS nanoparticles, which corresponds to $\approx 6.0 \times 10^9$ particles per mL and 1.0×10^8 particles per mL, as the final concentration of SARS-CoV-2 and HCoV-229E, respectively, in the stock inoculum and used as a reference in subsequent experiments.

3.5. Detection of SARS-CoV-2 Virus With Anti-Fouling Modification

After analyzing the anti-fouling effect of MESNA and quantification of SARS-CoV-2 virus titre, SARS-CoV-2 detection was
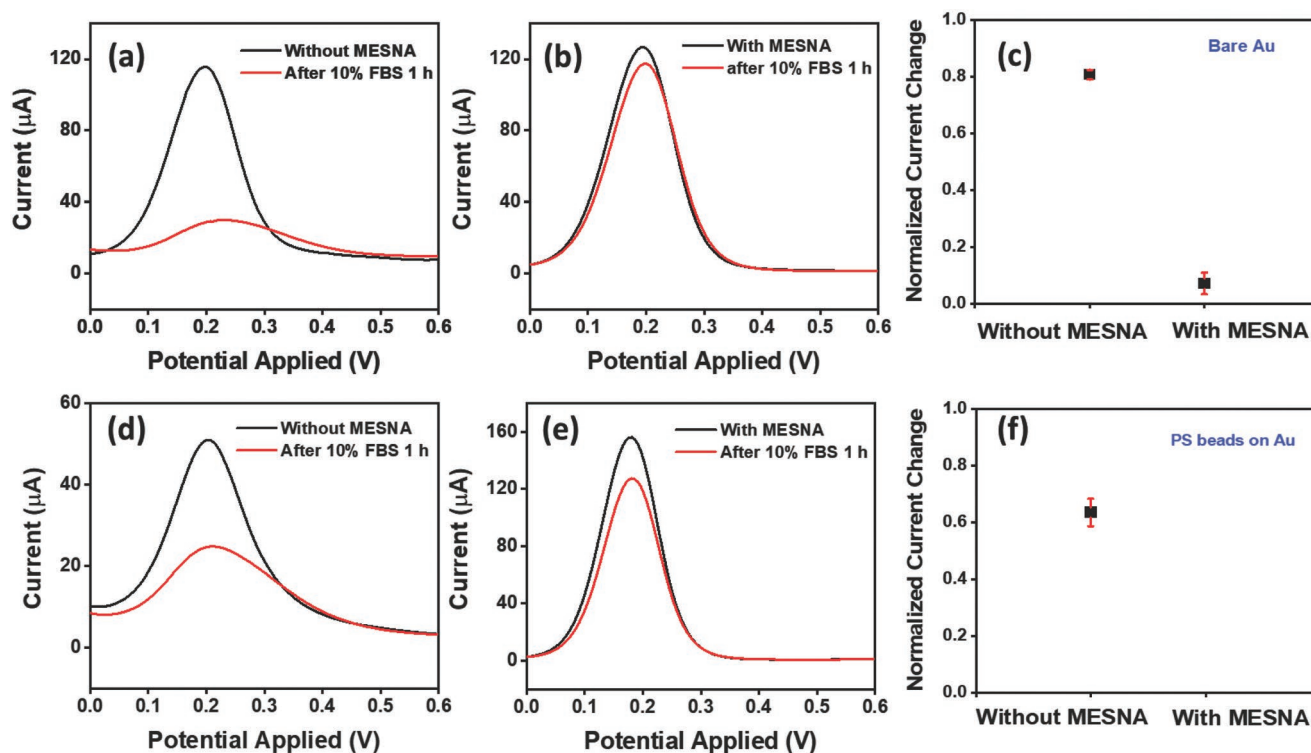
Figure 2. Evaluation of anti-fouling performance contributed by the introduction of the MESNA molecule. Comparison of DPV signals a) at the bare Au surface and b) the MESNA modified Au surface after 1 h incubation with pure PBS buffer (black line) and 10% FBS (red line). c) Comparison of the normalized oxidation current changes observed at the surface of bare Au electrodes and MESNA modified Au electrodes after 1 h incubation with pure PBS and 10% FBS. The error bars were generated from three measurements using three different electrodes. Comparison of DPV signals at PS beads coated Au surface d) without and e) with MESNA modification after 1 h incubation with PBS buffer (black line) and 10% FBS (red line). f) Comparison of the normalized oxidation current changes observed at the surface of PS beads coated Au electrodes without and with MESNA modification after 1 h incubation with pure PBS and 10% FBS. The error bars were generated from three measurements using three different electrodes.

carried out with MESNA modified biosensor in cell culture media. For this experiment, the biosensor was also challenged with another coronavirus strain (HCoV-229E) which has a similar morphology to SARS-CoV-2 (Figure S12, Supporting Information) and is responsible for seasonal cold. The virus inoculums were prepared by serial dilution of the stock inoculum with the same cell culture medium. As seen in the **Figure 3**a–c; although there was almost no change in DPV oxidation current in the biosensor treated with HCoV-229E, successive current decreases were observed in the biosensor tested with SARS-CoV-2 with increasing virus titre. The dosage response curves of SARS-CoV-2 and HCoV-229E presented in Figure 3d indicate that the biosensor can detect SARS-CoV-2 selectively and down to a concentration of 1.0 virus particle mL^{-1} in cell culture media. The sensitivity of the biosensor which corresponds to the slope of the dosage response curve was calculated to be $y = 0.0297x - 0.4$ ($R^2 = 0.9605$). The sensitivity of the biosensor was lower than for the previous experiment where the virus inoculum was diluted with DPBS (Figure 1d) possibly due to the screening to biofouling effect or the introduction of MESNA on the Au surface. The LOD of this biosensor was calculated using the equation: LOD = 3Sb1/slope where Sb1 is the standard deviation of the blank.[34] The MESNA modified nanochannel-based biosensor showed the LOD of 0.97 (≈1.0) virus particle mL^{-1} in cell culture media.

3.6. Detection of SARS-CoV-2 Virus in Clinical Samples

We further tested the capability of the MESNA modified nanochannel-based biosensors to detect SARS-CoV-2 virus in clinical samples. Human saliva samples from healthy volunteers were collected and divided into two groups: one group was spiked with SARS-CoV-2 virus particles to a final concentration of 10^4 virus particles per mL as the positive samples while the other group remained untreated as the negative samples. To remove cell debris and other large biomolecules, both the positive and negative samples were then subjected to two steps of filtration by using filter papers with a pore size of ≈1–3 μm first and 0.45 μm, subsequently. The filtered saliva samples were diluted by PBS buffer at 1:1 (v:v) and incubated with the stabilized biosensors. The results show that although both the positive samples and negative samples caused DPV oxidation signal decrease (**Figure 4**a,b), a statistically significant higher current drop was induced upon incubation with the positive samples compared to negative samples (Figure 4c), demonstrating that the nanochannel-based biosensors are capable of effectively distinguishing saliva samples containing the SARS-CoV-2 virus from those not containing the virus, allowing the effective differentiation between infected and non-infected patients.
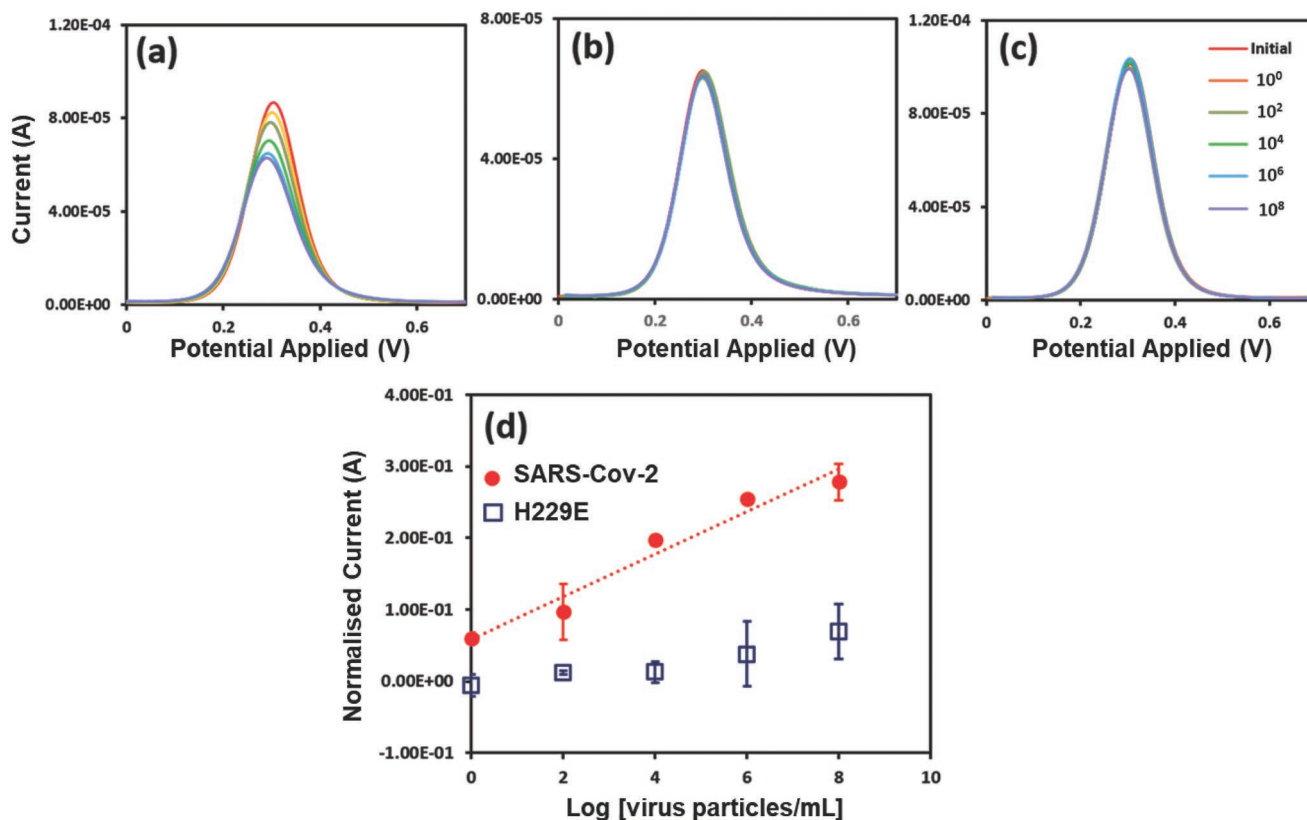
**ADVANCED
SCIENCE NEWS**

www.advancedsciencenews.com

NANO · MICRO

small

www.small-journal.com

Figure 3. DVPs of the biosensor upon consecutive incubations of a) SARS-CoV-2 virus inoculum diluted with cell culture media at a series of concentrations from 10^0 to 10^8 virus particles mL^{-1}, b) blank cell culture medium, and c) HCoV-229E virus diluted with cell culture media at a series of concentrations from 10^0 to 10^8 virus particles mL^{-1}. d) Dosage response curves of the biosensors incubated with consecutive dilutions of SARS-CoV-2 and HCoV-229E virus inoculum with cell culture medium.

4. Conclusion

Here, we reported a new strategy for SARS-CoV-2 virion detection in saline buffer and complex matrices (cell culture medium and human saliva) by using a nanochannel-based electrochemical biosensor modified by an antifouling molecule (MESNA). The nanochannels were constructed by PS microbeads (500 nm in diameter) which were uniformly coated on the Au electrode

by convective assembly. Further coating of SiO_2 as the passivation layer at a tilted angle contributed to the high sensitivity and an excellent LOD of the biosensor (≈1.0 virus particle mL^{-1}). In addition, the ability of the nanochannel biosensor to selectively detect SARS-CoV-2 virus particles in comparison to T4 phages and 229E coronavirus (which have a similar size to SARS-CoV-2 in cell culture medium) was demonstrated. The introduction of the antifouling biomolecule MESNA enhanced the stability and
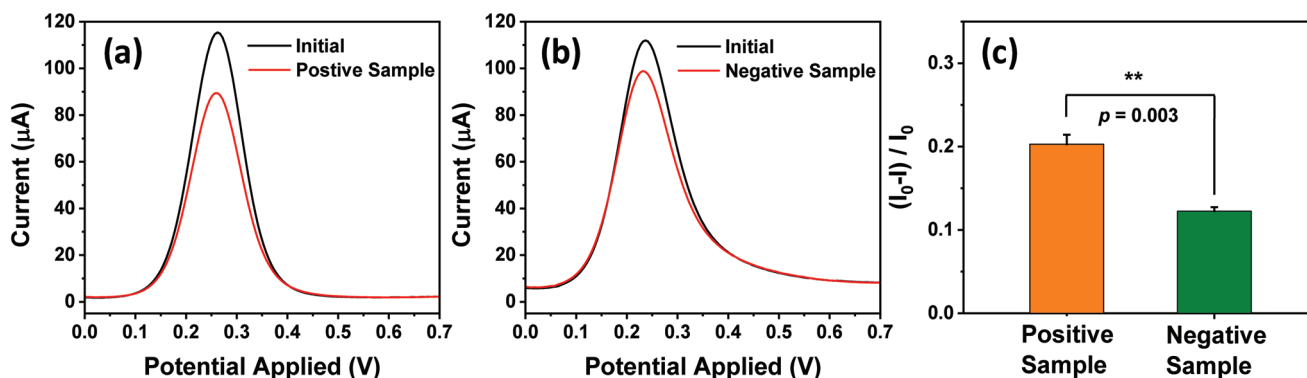

Figure 4. DPVs generated from a) the positive samples (saliva spiked with SARS-CoV-2 virus particles to a final concentration of 10^4 virus particles mL^{-1}) and from b) the negative sample (saliva without SARS-CoV-2 virus). c) Comparison of the normalized current changes measured from the positive samples and negative samples ($n = 3$). Data are presented as mean ± SD. Statistical analysis was performed using one-way ANOVA (*$p < 0.05$, **$p < 0.01$, and ***$p < 0.001$).

selectivity of the detection of target virus in the presence of foulants in cell culture media. Last, we demonstrated the capability of the biosensor to successfully differentiate between saliva samples containing the SARS-CoV-2 virus and those not containing the virus, allowing the effective differentiation between infected and non-infected patients. Overall, our cost-effective and unique biosensor fabrication strategy could be applied to a broad range of applications, such as the detection of other pathogenic viruses by tuning the pore size of the nanochannels and functionalizing corresponding bioreceptors.

Supporting Information

Supporting Information is available from the Wiley Online Library or from the author.

Conflict of Interest

The authors declare no conflict of interest.

Data Availability Statement

The data that support the findings of this study are available from the corresponding author upon reasonable request.

[1] S. Boopathi, A. B. Poma, P. Kolandaivel, *J. Biomol. Struct. Dyn.* **2021**, *39*, 3409.
[2] N. Reta, C. P. Saint, A. Michelmore, B. Prieto-Simon, N. H. Voelcker, *ACS Appl. Mater. Interfaces* **2018**, *10*, 6055.
[3] S. Toze, *Water Res.* **1999**, *33*, 3545.
[4] Y. Chai, D. Tian, W. Wang, H. Cui, *Chem. Commun.* **2010**, *46*, 7560.
[5] Y. Boum, K. N. Fai, B. Nikolay, A. B. Mboringong, L. M. Bebell, M. Ndifon, A. Abbah, R. Essaka, L. Eteki, F. Luquero, C. Langendorf, N. F. Mbarga, R. G. Essomba, B. D. Buri, T. M. Corine, B. T. Kameni, N. Mandeng, M. Fanne, A. C. Z. K. Bisseck, C. B. Ndongmo, S. Eyangoh, A. Hamadou, J. P. Ouamba, M. T. Koku, R. Njouom, O. M. Claire, L. Esso, E. Epée, G. A. E. Mballa, *Lancet Infect. Dis.* **2021**, *21*, 1089.
[6] R. W. Peeling, P. Olliaro, *Lancet Infect. Dis.* **2021**, *21*, 1052.
[7] N. Reta, A. Michelmore, C. Saint, B. Prieto-Simón, N. H. Voelcker, *Biosens. Bioelectron.* **2016**, *80*, 47.
[8] L. Reverté, B. Prieto-Simón, M. Campàs, *Anal. Chim. Acta* **2016**, *908*, 8.
[9] M. Negahdary, *Biosens. Bioelectron.* **2020**, *152*, 112018.
[10] S. A. Zaidi, J. H. Shin, *Talanta* **2016**, *149*, 30.
[11] G. Rajeev, B. Prieto Simon, L. F. Marsal, N. H. Voelcker, *Adv. Healthcare Mater.* **2018**, *7*, 1700904.
[12] N. Reta, A. Michelmore, C. P. Saint, B. Prieto-Simon, N. H. Voelcker, *ACS Sens.* **2019**, *4*, 1515.
[13] A. de la Escosura-Muñiz, M. Espinoza-Castañeda, A. Chamorro-García, C. J. Rodríguez-Hernández, C. de Torres, A. Merkoçi, *Biosens. Bioelectron.* **2018**, *107*, 62.
[14] A. de la Escosura-Muñiz, W. Chunglok, W. Surareungchai, A. Merkoçi, *Biosens. Bioelectron.* **2013**, *40*, 24.
[15] A. De La Escosura-Muñiz, A. Merkoçi, *Small* **2011**, *7*, 675.
[16] G. Rajeev, E. Melville, A. J. Cowin, B. Prieto-Simon, N. H. Voelcker, *Front Chem* **2020**, *8*, 155.
[17] K. Guo, A. Sharma, R. J. Toh, E. Alvárez de Eulate, T. R. Gengenbach, X. Cetó, N. H. Voelcker, B. Prieto-Simón, *Adv. Funct. Mater.* **2019**, *29*, 1809206.
[18] A. Shiohara, C. D. Easton, B. Prieto-simon, N. H. Voelcker, *Biosensors* **2022**, *12*, 480.
[19] V. M. Corman, O. Landt, M. Kaiser, R. Molenkamp, A. Meijer, D. K. W. Chu, T. Bleicker, S. Brünink, J. Schneider, M. L. Schmidt, D. G. J. C. Mulders, B. L. Haagmans, B. Van Der Veer, S. Van Den Brink, L. Wijsman, G. Goderski, J. L. Romette, J. Ellis, M. Zambon, M. Peiris, H. Goossens, C. Reusken, M. P. G. Koopmans, C. Drosten, *Euro Surveill.* **2020**, *25*, 2000045.
[20] N. A. Fleck, R. M. McMeeking, T. Kraus, *Langmuir* **2015**, *31*, 13655.
[21] C. D. Easton, C. Kinnear, S. L. McArthur, T. R. Gengenbach, *J. Vac. Sci. Technol.* **2020**, *38*, 023207.
[22] A. Fokine, V. D. Bowman, A. J. Battisti, Q. Li, P. R. Chipman, V. B. Rao, M. G. Rossmann, *Virology* **2007**, *367*, 422.
[23] M. Ghallab, C. Barsoum, S. Polak, E. Hassoun, O, A. G. , *Bratisl. Lek. Listy* **2021**, *122*, 900.
[24] R. Yang, Q. He, C. Wang, S. Sun, *Ferroelectrics* **2018**, *530*, 130.
[25] A. N. Yusilawati, M. Maizirwan, I. Sopyan, M. S. Hamzah, K. H. Ng, C. S. Wong, *Adv. Mater. Res.* **2011**, *264–265*, 1532.
[26] K. Aslan, C. C. Luhrs, V. H. Pérez-Luna, *J. Phys. Chem. B* **2004**, *108*, 15631.
[27] M. Ali, B. Schiedt, R. Neumann, W. Ensinger, *Macromol. Biosci.* **2010**, *10*, 28.
[28] X. Chen, A. Noy, *APL Mater.* **2021**, *9*, 020701.
[29] E. Ostuni, R. G. Chapman, M. N. Liang, G. Meluleni, G. Pier, D. E. Ingber, G. M. Whitesides, *Langmuir* **2001**, *17*, 6336.
[30] A. K. Nowinski, F. Sun, A. D. White, A. J. Keefe, S. Jiang, *J. Am. Chem. Soc.* **2012**, *134*, 6000.
[31] M. Cui, Y. Wang, H. Wang, Y. Wu, X. Luo, *Sens. Actuators, B* **2017**, *244*, 742.
[32] T. Christoff-tempesta, E. Deiss-yehiely, P. C. Dromel, L. D. Uliassi, C. A. C. Chazot, E. Postelnicu, A. J. Hart, M. Spector, P. T. Hammond, J. H. Ortony, *Adv. Mater. Technol.* **2022**, *9*, 2200311.
[33] W. Zhao, Q. Ye, H. Hu, X. Wang, F. Zhou, *RSC Adv.* **2015**, *5*, 100347.
[34] H. Gu, N. Duan, Y. Xia, X. Hun, H. Wang, Z. Wang, *J. Agric. Food Chem.* **2018**, *66*, 9801.